Anatomy of an Earthquake Early Warning (EEW) Alert: Predicting Time Delays for an End-to-End EEW System

by Yannik Behr, John Clinton, Philipp Kästli, Carlo Cauzzi, Roman Racine, and Men-Andrin Meier

INTRODUCTION

Earthquake early warning (EEW) systems can play an important role in seismic-risk mitigation, filling the gap between long-term measures such as earthquake safe building design (e.g., Housner *et al.*, 1997) and medium-to-short term measures like operational earthquake forecasting (e.g., Gerstenberger *et al.*, 2005) and rapid notifications following a strong earthquake (e.g., Wald *et al.*, 1999). Throughout the last two decades algorithmic improvements, denser seismic networks, and new communication technologies have made EEW feasible. With the achievable warning times increasing continuously, EEW is becoming useful to a wider range of potential end users (Böse *et al.*, 2013).

EEW algorithms can roughly be grouped into three categories: on-site, regional, and front detection approaches. The on-site approach sends an alert when one or more thresholds of waveform parameters measured in real time are exceeded at one or two stations (Nakamura, 1988; Kanamori, 2005; Böse, Hauksson, Solanki, Kanamori, and Heaton, 2009). The regional approach waits for the earthquake to be detected at a number of sites to estimate its location and then uses an empirical relationship to infer the magnitude and expected ground motion at a target site from the first few seconds of waveforms (Allen and Kanamori, 2003; Cua and Heaton, 2007; Cua *et al.*, 2009; Satriano *et al.*, 2011). The front detection approach is a special case of a regional approach that targets a specific area known to generate strong seismicity, hence the origin is assumed and only the magnitude is inferred (e.g., Espinosa-Aranda *et al.*, 1995; Mărmureanu *et al.*, 2011). Usually seismicity cannot be assumed to only occur in a particular area, and therefore the majority of operational and in-development EEW algorithms today run an implementation of the onsite approach (Nakamura *et al.*, 2011) or, more commonly, a combination of the on-site and network-based regional algorithms (Hoshiba *et al.*, 2008; Hsiao *et al.*, 2011; Böse *et al.*, 2013; Zollo *et al.*, 2013) that use dense seismic networks to provide warnings from distributed seismicity to distributed populations. In several countries, such as Japan, China, Taiwan, Mexico, Turkey, and Romania, EEW systems are already operational; in other regions, such as the U.S. west coast, southern Italy, or Switzerland, EEW algorithms are in the prototype phase (Allen *et al.*, 2009).

The performance of these algorithms is usually measured in terms of delay time between the earthquake occurrence and the first issued alert and of the accuracy of the corresponding earthquake source parameter estimates or the predicted ground motion. There is an intrinsic trade-off between the accuracy and the speed of an alert. Onsite algorithms are usually faster but tend to have a lower accuracy, whereas regional algorithms are slower but more accurate (Kanamori, 2005). In this study, we focus on the detailed analysis of delay times in a regional EEW system, the Virtual Seismologist (VS; Cua and Heaton, 2007). Our proposed methodology for analyzing delays, however, is transferable to any of the currently operational regional EEW algorithms and, with minor modifications, also to onsite algorithms.

The delay times for different EEW algorithms have been analyzed before; for example, Brown *et al.* (2011) and Kuyuk *et al.* (2014) discussed delay times for the Earthquake Alarm System (ElarmS) in California, including datalogger and pre-processing latencies. Böse, Hauksson, Solanki, Kanamori, and Heaton (2009) analyzed delay times of the Onsite early warning algorithm in southern California, and Satriano *et al.* (2011) presented a similar study for the PRobabilistic and Evolutionary early warning SysTem (PRESTo) in southern Italy, running on the Irpinia Seismic Network.

These studies used real seismicity to assess the performance of the respective algorithms, which provides a partial overview limited to areas where earthquakes occurred during the testing of the algorithm. Heaton (1985), Allen (2006), Kuyuk and Allen (2013), and Auclair *et al.* (2014) used hypothetical hypocenters either distributed evenly across a certain area or along known faults to describe warning time scenarios, assuming a constant time delay for data transmission and processing. All EEW system components add a delay to the overall alert time; and, more importantly, these delays show fluctuations for different times and different parts of the network. Assuming constant delays, therefore, cannot accurately explain all alert times observed in a real-time system. With speed being the dominant factor in EEW, understanding the contribution of each component in an EEW system to the overall delay of an alert is crucial to identify the weakest components of an EEW architecture and thereby make improvements with the highest

impact. In this study, we extend previous work on EEW performances by assuming a homogeneous distribution of earthquakes combined with detailed measurements of delay times and the network geometry to estimate the alert times from our regional EEW algorithm at any point within a given area. We verify our model of expected alert times by comparing it with the observed initial alert times for seismicity within the model boundaries. Our analysis allows us to reliably predict the expected delay and its error bounds between the earthquake origin time and the first alert for any hypothetical epicenter within the region of interest. Hence, our work fills the gap between studies analyzing real-time delays for selected events and those modeling alert times for hypothetical events, assuming constant system delays. Our results not only provide a reliable estimate of performance to potential end users of EEW alerts, but also could be extended to compare alert times of different EEW algorithms running on the same seismic network.

DEFINING DELAYS IN AN EEW SYSTEM

Currently all operational regional EEW algorithms consist of similar basic system components for detecting first arrivals on the waveforms, event association, and location; for estimating magnitude, given the epicenter; and for predicting ground motion at a target site, given magnitude and epicenter. The algorithms only differ in how the location, magnitude, and ground motion are estimated. We take advantage of the similarities to propose a definition of delays for an EEW system that is specific to one algorithm but could be applied generically. Most operational EEW systems then compute ground motion from the magnitude, epicenter, and the distance to the target site by applying a ground-motion prediction equation. Because this computation is almost instantaneous, we will not discuss it further in the context of delay times.

The EEW algorithm we use for this analysis is the VS (Cua and Heaton, 2007; Cua et al., 2009), a Bayesian approach to regional network-based EEW. It has been implemented as a real-time product at the Swiss Seismological Service since 2006; and, since 2008, it has been running in real time as one of the three EEW algorithms that comprise the California Integrated Seismic Network (CISN) ShakeAlert demonstration system in California—the other two being ElarmS (Allen and Kanamori, 2003; Allen, 2007; Brown et al., 2011; Kuyuk et al., 2014) and Onsite (Kanamori, 2005; Wu et al., 2007; Böse, Hauksson, Solanki, Kanamori, Wu, et al., 2009; Böse, Hauksson, Solanki, Kanamori, and Heaton, 2009). There are currently two real-time implementations of VS, which are based on the same equations to estimate the magnitude (Cua and Heaton, 2007) but use different association and location algorithms. The version operational in Switzerland since early 2013 is implemented as a set of modules in the SeisComP3 system (Hanka et al., 2010) and referred to as VS(SC3). In California, VS uses parts of the Earthworm system (referred to as VS(EW); http://www.earthwormcentral.org; last accessed 16 December 2014). In practice, the most important differences are (1) VS(SC3) requires six detections for an initial location, whereas VS(EW) starts searching for a location with four detections; (2) VS(SC3) uses both broadband and strong-motion stations for location and magnitude estimates, whereas VS(EW) only uses broadband stations; and (3) VS(SC3) uses a minimum of 3 s waveform data in order to estimate magnitude, whereas VS(EW) uses 1 s. Differences between the two systems could be reduced through configuration changes and additional software development. Our focus in this study, however, lies in the accurate description of delays in these systems rather than their optimization. Studying delays in both the Swiss and the Californian system, where different network geometry, hardware, telemetry, and software are used, demonstrates that our analysis can be applied to different EEW systems.

The time between the nucleation of an earthquake and the issuance of the first alert can be split into the following components:

$$\Delta t_{\mathrm{origin}} = \max(\overrightarrow{\Delta t_P} + \overrightarrow{\Delta t_t}) + \Delta t_a \qquad (1.1)$$

and

$$\Delta t_{\mathrm{alert}} = \max[\min(\overrightarrow{\Delta t_p} + \overrightarrow{\Delta t_w}), \Delta t_{\mathrm{origin}}] + \Delta t_m + \Delta t_d. \qquad (1.2)$$

Figure 1 illustrates equations (1.1) and (1.2), and Table 1 gives a summary of the delay times and their various dependencies that we will discuss in more detail in the following paragraphs.

Equation (1.1) provides the component delays involved in estimating the earthquake origin ($\Delta t_{\mathrm{origin}}$ is the time difference between the earthquake origin time and the first hypocenter estimate), and equation (1.2) provides the component delays
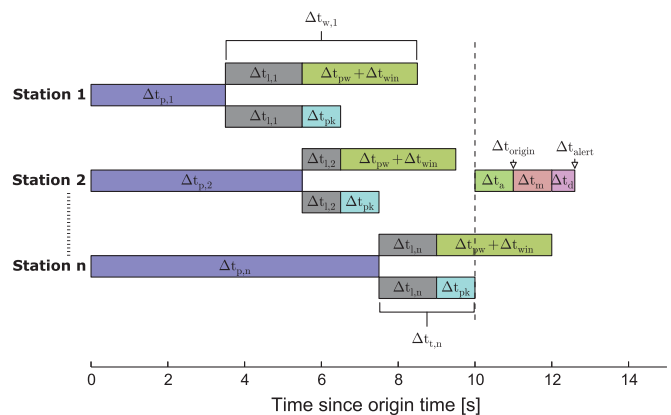
▲ **Figure 1.** Summary of the delays that are part of an earthquake early warning (EEW) alert. See Table 1 for definitions of the delay components. The lengths of the bars are representative of the delays measured in the Swiss seismic network and VS(SC3). The vertical dashed line marks the time when enough *P*-wave arrivals are detected to start computing a hypocenter estimate. In the displayed example, station n does not contribute to the magnitude estimate because insufficient waveform data are available at the time of the first location estimate ($\Delta t_{\mathrm{origin}}$).

Table 1
Detailed Description of the Different Delay Components Described in the Defining Delays in an EEW System section, Including Information on What Factor the Delays Depend on and How They are Measured in This Study

Delay	Description	Dependencies	Measurement
Δt_{alert}	Time between an event's origin time and the arrival of the EEW alert at the target site	$\overrightarrow{\Delta t_P}, \overrightarrow{\Delta t_t}, \overrightarrow{\Delta t_w}, \Delta t_a,$ $\Delta t_m, \Delta t_d$	Event log files (Using Observed Delays to Model Expected Alert Times section)
Δt_{origin}	Time between an event's origin time and the first available hypocenter estimate	$\overrightarrow{\Delta t_P}, \overrightarrow{\Delta t_t}, \Delta t_a$	Not measured explicitly
$\overrightarrow{\Delta t_P}$	Travel time of the P wave to the first n stations	Network geometry and hypocentral location	Synthetic travel times (P-Wave Travel Time ($\overrightarrow{\Delta t_P}$) section)
$\overrightarrow{\Delta t_t}$	Time difference between the arrival of the P wave at the first n stations and the trigger/detection of the P wave	$\overrightarrow{\Delta t_l}, \Delta t_{pk}$	Continuous log files (Trigger Delays ($\overrightarrow{\Delta t_t}$) section)
$\overrightarrow{\Delta t_l}$	Data latency for each of the first n stations	$\overrightarrow{\Delta t_{\text{log}}}, \overrightarrow{\Delta t_{\text{trans}}}, \Delta t_{\text{rec}}$	Continuous log files (Data Latency ($\overrightarrow{\Delta t_l}$) section)
$\overrightarrow{\Delta t_{\text{log}}}$	Processing and packaging at the datalogger at the first n stations	Datalogger type and configuration (e.g., sampling rate)	Not measured independently
$\overrightarrow{\Delta t_{\text{trans}}}$	Telemetry delay between the first n stations and the datacenter	Communications, sampling rate	Not measured independently
Δt_{rec}	Receiver queuing and processing delay at the datacenter	Acquisition software	Not measured independently
Δt_{pk}	Processing delay of the automatic picker	EEW software	Not measured independently
Δt_a	Processing delay of the associator to locate and declare an event using the first n P-wave detections	EEW software	Event log files (Associator Delay (Δt_a) section)
$\overrightarrow{\Delta t_w}$	Time between the arrival of the P wave at each of the first n stations and when k seconds of waveform data are available in order to estimate the magnitude.	$\overrightarrow{\Delta t_l}, \Delta t_{\text{win}}(k), \Delta t_{pw}$	Continuous log files (Waveform Delays ($\overrightarrow{\Delta t_w}$) section)
$\Delta t_{\text{win}}(k)$	Waveform window, k seconds long	EEW software	Configuration setting
Δt_{pw}	Preprocessing of waveform data	EEW software	Not measured independently
Δt_m	Processing delay to compute the EEW magnitude with the available location and waveform data	EEW software	Event log files (Magnitude Estimation Time (Δt_m) section)
Δt_d	Telemetry delay to disseminate an alert	Messaging system and end-user internet connection	Not measured here

involved in providing the EEW alert (Δt_{alert} is the time difference between the origin time and the issuance of the first alert).

The first delay in equation (1.1) ($\max(\overrightarrow{\Delta t_P} + \overrightarrow{\Delta t_t})$) reflects the fact that an earthquake origin depends on the time for seismic P waves to travel from the hypocenter to the minimum number of seismic stations ($\overrightarrow{\Delta t_P}$) and the consequent time required for the relevant part of waveform that includes the P-wave energy to be transmitted to a processing hub and a detection to be made on the data ($\overrightarrow{\Delta t_t}$; referred to as the trigger delay). Different seismic stations may have different hardware, datalogger, or telemetry configurations, so the station closest to the epicenter may not produce the earliest detection at the processing hub. The second delay in equation (1.1) is the time taken to estimate the hypocenter once sufficient detections are available (Δt_a).

In equation (1.2), the first part ($\max[\min(\overrightarrow{\Delta t_P} + \overrightarrow{\Delta t_w}), \Delta t_{\text{origin}}]$) reflects the requirement that before an event

magnitude can be estimated, both an earthquake hypocenter (Δt_{origin}) and a sufficient duration of postdetection waveform data are available at least at one station. The time needed to collect the required data for magnitude estimation at the processing hub depends on both the time it takes the seismic data to travel from the hypocenter to the required number of stations ($\overrightarrow{\Delta t_P}$) and the consequent time required to assemble the data for magnitude estimation ($\overrightarrow{\Delta t_w}$; referred to as the waveform delay). To start estimating the magnitude, k seconds of waveform data following the P-wave detection at one station ($\Delta t_{\text{win}}(k)$) are sufficient, and therefore the first magnitude estimate will come from the stations for which this waveform window is first available at the processing hub ($\min(\overrightarrow{\Delta t_P} + \overrightarrow{\Delta t_w})$) once a first location estimate has been computed. In the case of VS, the data are converted into ground-motion envelopes for each component in terms of ac-

celeration, velocity, and displacement, and the peak parameters for each are tracked. This adds a small preprocessing delay (Δt_{pw}) to $\overrightarrow{\Delta t_w}$. $\Delta t_{win}(k)$ is 1 or 3 s, depending on the VS algorithm configuration. Included in $\overrightarrow{\Delta t_w}$ is also the data latency between the stations and the processing hub ($\overrightarrow{\Delta t_l}$). The original VS algorithm requires at least 3 s of waveform data following a P-wave trigger to compute the magnitude. In VS(EW), this requirement was relaxed to 1 s of waveform data. Although this does not strictly follow the original algorithm, in most cases Δt_{origin} is long enough that at least 3 s of waveform data will be available at a number of stations once a first epicenter estimate is available. In the few cases when Δt_{origin} is less than $\min(\overrightarrow{\Delta t_p} + \overrightarrow{\Delta t_w})$, the initial alert will likely underestimate the magnitude. The later parts of equation (1.2) add the time taken to determine the magnitude for the given hypocenter and the related solution uncertainties (Δt_m), and the consequent time taken to disseminate an alert (Δt_d).

An important part of the system is the data latency for each station i in the network ($\Delta t_{l,i}$) which contributes to delays in both the hypocentral ($\overrightarrow{\Delta t_t}$) and magnitude ($\overrightarrow{\Delta t_w}$) estimation. The data latency at station i, $\Delta t_{l,i}$, can be split up into the delay introduced by the datalogger $\Delta t_{log,i}$, the transmission delay $\Delta t_{trans,i}$ of the communications system, and the receiver queuing and processing delay Δt_{rec} ($\Delta t_{l,i} = \Delta t_{log,i} + \Delta t_{trans,i} + \Delta t_{rec}$; Steim and Reimiller, 2014). $\Delta t_{log,i}$ includes the length of each data packet (usually dependent on sampling rate but often also the proprietary datalogger characteristics), real-time filter operations, and data transmission modes. The trigger delay at station i ($\Delta t_{t,i}$) is the sum of the data latency for this station ($\Delta t_{l,i}$) and Δt_{pk}, the time required to detect a P-wave arrival once the waveform data have arrived.

The main part of this article deals with measuring these delays and evaluating how they contribute to an EEW alert delay. For various reasons, it is impractical to measure each delay independently using exactly the same dataset. Some elements (e.g., data latency) can be continuously recorded in the absence of events but only for short periods of time due to the large number of measurements they produce; other elements can only be measured during event occurrence, hence measuring them can only be done during infrequent earthquakes but over long timespans.

Our delay analysis mixes observations from real-time operations and offline playbacks. In theory, only the parameters $\overrightarrow{\Delta t_l}$ and Δt_d should differ between real-time and playback modes. In practice, however, it proves to be difficult to separate the parameters $\Delta t_{win}(k) + \Delta t_{pw}$ and Δt_{pk} from $\overrightarrow{\Delta t_l}$ and we, therefore, measured in addition to $\overrightarrow{\Delta t_l}$ also $\overrightarrow{\Delta t_t}$ and $\overrightarrow{\Delta t_w}$ during real-time operations. Steim and Reimiller (2014) described a method to accurately measure $\overrightarrow{\Delta t_l}$ for the case of a popular datalogger (Quanterra Q330). They pointed out that measuring time delays accurately by simply measuring the difference between the timestamp of a data point and its arrival at the datacenter requires well-synchronized clocks at both ends. Despite this obvious drawback, this appears to be the best solution for networks with different dataloggers, not all of which have the capability to produce synthetic test signals like the Q330 dataloggers. We therefore define the data latency as the difference between the timestamp of a data sample in a data package and the arrival of the data package at the processing system. $\overrightarrow{\Delta t_t}$ and $\overrightarrow{\Delta t_w}$ were measured similarly as the difference between recording of the signal at the datalogger and the creation time of a pick and an envelope value at the processing hub.

We measured Δt_m from offline playbacks of archived waveform data, and $\overrightarrow{\Delta t_P}$ was estimated using travel times computed in a homogeneous half-space. In Switzerland, the SeisComP3 system has routinely recorded Δt_a in real time since October 2012, when the Swiss Seismological Service changed to SeisComP3 as its earthquake monitoring system. In California, we measured Δt_a from offline playbacks.

The alert dissemination time Δt_d, which is the delay between the issuance of an alert and the arrival at the recipient, depends on the Internet connection of the recipient and therefore cannot be measured reliably. However, delays introduced by the underlying messaging system (ActiveMQ; http://activemq.apache.org/; last accessed 16 December 2014) are typically on the order of ≤0.1 s (Ivan Henson, personal comm., 2014), which is small enough to not be considered in this study.

Offline playbacks were performed by feeding archived waveform data into the EEW system, mimicking the real-time processing. In this process, we simulated data latencies (Δt_l) by either assuming a constant but individual delay for every station in the network (for VS(SC3)) or by delaying the data from every station by the same amount (for VS(EW)).

DELAY ANALYSIS

This section includes a detailed analysis of key delay measurements.

P-Wave Travel Time ($\overrightarrow{\Delta t_P}$)

Δt_P describes the time elapsed before an earthquake is detected by a sufficient number of sensors in order to be locatable. In Figures 2 and 3, we show the theoretical time taken for earthquakes to be detected by sensors operated in the dense seismic networks in Switzerland and California. We assumed epicenters are homogeneously distributed with a hypocentral depth of 8 km and a homogeneous P-wave velocity of 6.5 km/s. A more realistic velocity model has minor impact because only the travel paths to stations closest to the epicenter are relevant.

Figure 2 shows the time required for the P wave to travel from any theoretical hypocenter to the first six seismic stations (the minimum number for VS(SC3)) in Switzerland, spanning the region within which the Swiss Seismological Service routinely locates earthquakes (Fäh et al., 2011; Diehl et al., 2013). In areas with increased network density (the Valais region in the south, Basel in the northwest, St. Gallen in the northeast, as well as central Switzerland and eastern Graubünden),
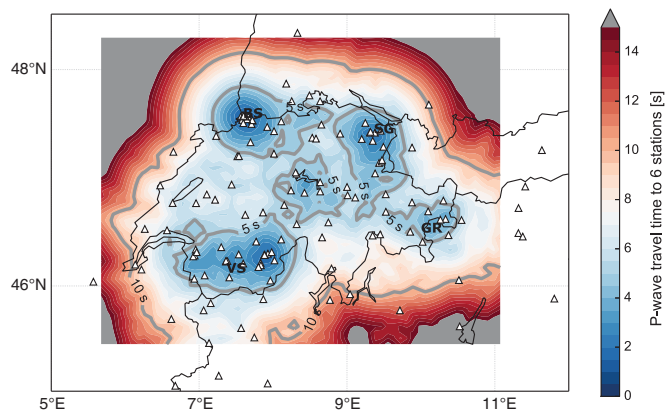
▲ **Figure 2.** Delay due to seismic network geometry in Switzerland. The color indicates the *P*-wave travel time to six seismic stations from any point within the colored area. White triangles mark the locations of broadband and strong-motion stations that stream data to the Swiss Seismological Service in real time, and gray lines mark the 5 and 10 s contours. BS, Basel; SG, St. Gallen; VS, Valais; GR, Graubünden.

$\max(\overrightarrow{\Delta t_P})$ is less than 5 s. For almost any other hypocenter location within Switzerland, $\max(\overrightarrow{\Delta t_P})$ is less than 10 s (see gray contour lines in Fig. 2).

Figure 3 shows the *P*-wave travel time to four real-time broadband stations (the minimum number in VS(EW)) for the CISN seismic network in California operated by the California Institute of Technology, the Berkeley Seismology Laboratory at the University of California at Berkeley (UC Berkeley), and the U.S. Geological Survey (USGS) at Menlo Park. The network geometry continuously changes, and we only included stations that were operational over the entire time period analyzed in this study (January 2012–December 2013). The gray contour line that marks the area with $\max(\overrightarrow{\Delta t_P})$ less than 5 s includes the San Francisco Bay and Mammoth Lakes area in northern California and some areas around the southern part of the San Andreas fault, including the Los Angeles basin in southern California. The 10 s contour surrounds the western part of southern California, the San Francisco Bay, the Mammoth Lakes area, and parts of the Eureka region in northern California. In the rest of the state and offshore, $\max(\overrightarrow{\Delta t_P})$ increases abruptly to values exceeding 15 s. In California, a separate instance of VS(EW) is running at each of the three network operators, each only seeing their respective part of the seismic network. As a result, parts of the network appear more sparse than they actually are. The inset in Figure 3 shows $\max(\overrightarrow{\Delta t_P})$ for the case in which all seismic networks are combined into a single statewide system.

The two figures show that even in dense networks, areas where station density declines can lead to rapid increases in delay times. These could be reduced by using single-station approaches, but network geometry will always play a key role in the delays seen by an EEW system.
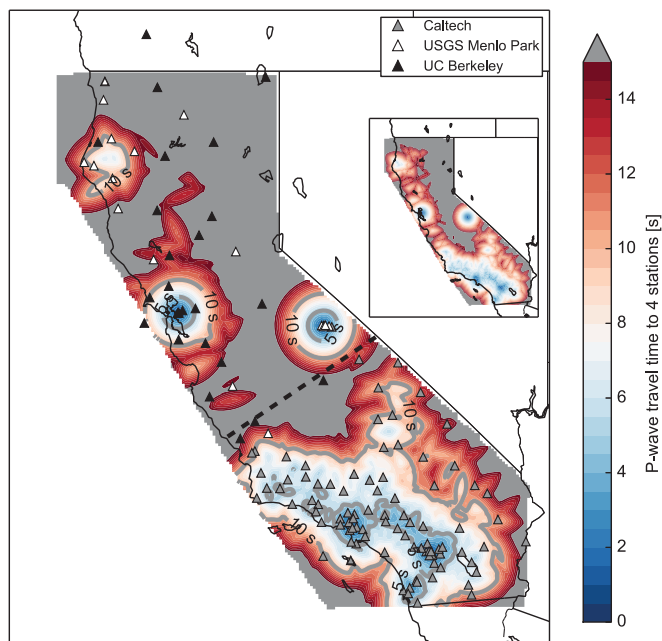

▲ **Figure 3.** Same as Figure 2 but for California; the color here indicates the *P*-wave travel time to only four broadband stations of the three seismic networks operated in California. Triangles mark the locations of real-time broadband stations, and gray lines mark the 5 and 10 s contours. The inset shows $\max(\overrightarrow{\Delta t_P})$ if all seismic networks in California are combined.

Data Latency $(\overrightarrow{\Delta t_l})$

The data latency describes the delay between the signal being recorded at the sensor/datalogger in the field and the arrival of the corresponding digitized waveform at the processing hub. It is mostly controlled by the type and configuration of the datalogger and the telemetry. We measured $\overrightarrow{\Delta t_l}$ for limited periods of time on continuous data independent of events.

Figure 4a shows $\Delta t_{l,i}$ for all real-time stations *i* within the Swiss seismic network (including broadband and strong-motion sensors) and stations for which real-time streams are provided by foreign partners.[1] Variations in delays are caused by (1) differences in dataloggers, sampling rates, and telemetry and (2) an additional relay or data conversion. For most of the neighboring networks, EEW is not a goal, so often no major attempt is made by these agencies to maximize the system speed. $\Delta t_{l,i}$ for the three different networks run in California are shown in Figure 4b. Stations monitored by the Berkeley Seismological Laboratory at UC Berkeley are equipped with dataloggers capable of sending 1 s data packets and therefore display the lowest latencies. The network operated by the

---
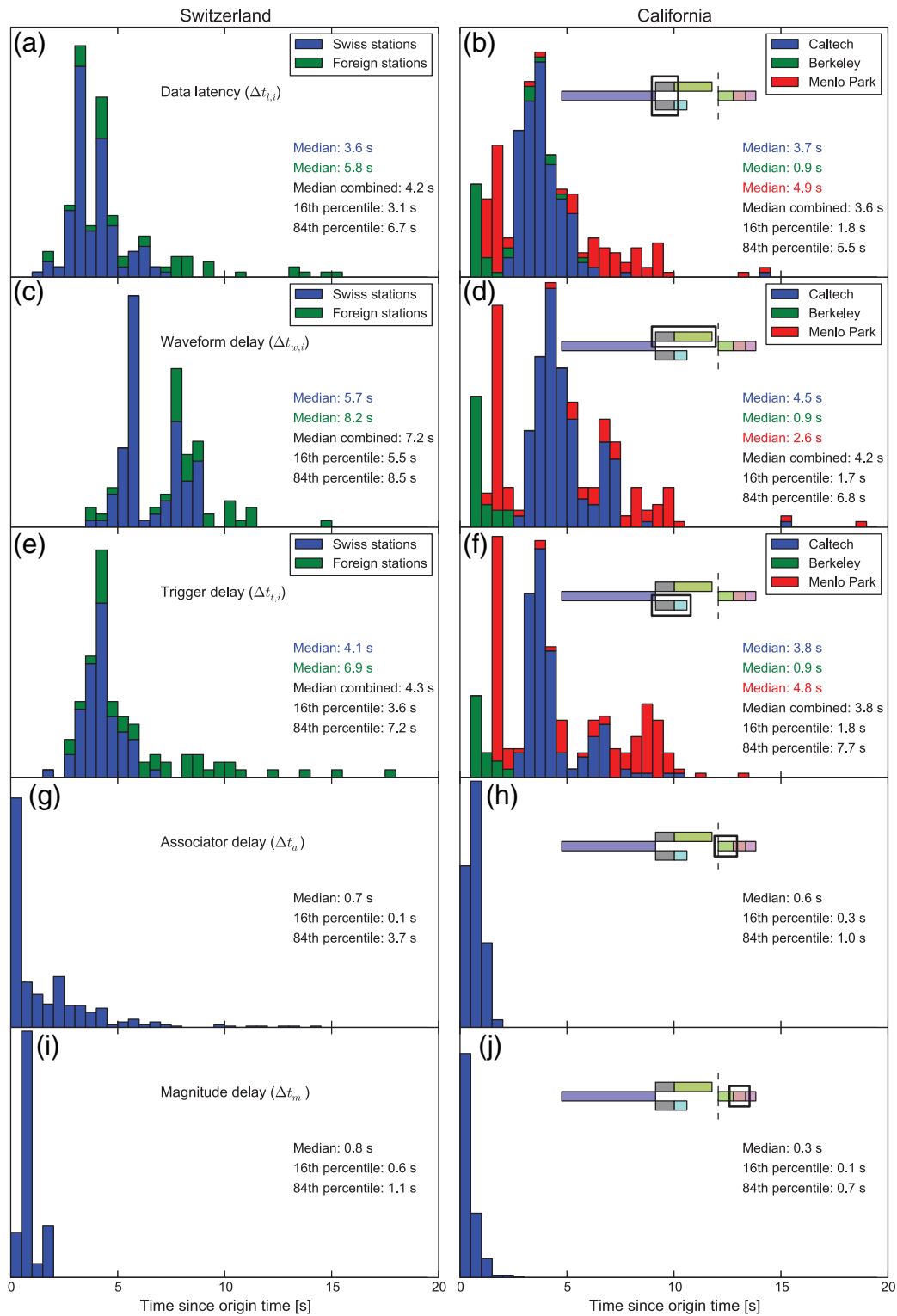
▲ **Figure 4.** Delay time summaries measured for VS(SC3) (a,c,e,g, and i for Switzerland) and VS(EW) (b,d,f,h, and j for California). The insets on b,d,f,h, and j show a simplified version of Figure 1, with the black box indicating the delay that is displayed in the respective subfigure. (a,b) The distribution of $\Delta t_{l,i}$ for all stations i sending data in real time to the Swiss and Californian networks, respectively; (c,d) $\Delta t_{w,i}$ measured during real-time operations; (e,f) the distribution of $\Delta t_{t,i}$; (g) the distribution of Δt_a measured in real time from 289 events with magnitude ≥1.5 that occurred in Switzerland and adjacent regions between October 2012 and October 2013; (h) same as (g) measured from offline playbacks of 119 events with magnitude ≥3.5 that occurred in southern California between January 2010 and August 2012; (i) t_m measured from offline playbacks of 97 events with magnitude ≥2.5 that occurred between January 2009 and June 2013 in Switzerland and adjacent regions; (j) same as (i) but measured from offline playbacks of the same 119 events as in (h). All histograms have been normalized.

USGS in Menlo Park is equipped with dataloggers not capable of sending 1 s data packets and uses slow telemetry solutions for some stations, resulting in median data latencies of around 5 s. Caltech stations used by VS(EW) have only recently been optimized to sending 1 s packets; therefore, in our analysis, stations in southern California show systematically larger latencies than those operated by UC Berkeley.

The distributions for $\Delta t_{l,i}$ (as well as for $\Delta t_{t,i}$, and $\Delta t_{w,i}$) in Figure 4 were truncated for clarity but continue beyond the limits with rare outliers. Kuyuk *et al.* (2014) showed that the datalogger upgrades for the seismic stations operated by UC Berkeley reduced median delay times by ~3 s, which directly translates into an ~3 s reduction of alert times for events within this network. Improvements of this scale can only be expected for significant algorithmic advances combined with a much higher station density. As a result, optimizing datalogger and telemetry configurations seems the most cost-effective measure to improve alert times.

Waveform Delays ($\overrightarrow{\Delta t_w}$)

The waveform delay is the time between the arrival of the P wave at a sensor and the time when enough waveform data are available at the processing hub to compute a first magnitude estimate. We measured it from continuous real-time data during a short time window (usually around 1 h) as the time difference between the recording of a waveform at the station and the arrival of k seconds of envelope values (for VS(SC3), $k = 3$; for VS(EW), $k = 1$) at the magnitude computation module following that recorded waveform.

The distribution of $\Delta t_{w,i}$ for all stations i in VS(SC3) (Fig. 4c) exhibits two maxima, roughly at ~4 and 8 s. This is due to the 3 s of data required for spanning single or multiple data packets. In the VS(EW) system in California, we do not see such a bimodal distribution, because in this system, magnitude estimation begins with the first second of waveform data (Fig. 4d). The strong similarities between Figure 4b and 4d again confirm that $\Delta t_{w,i}$ is dominated by $\Delta t_{l,i}$ and that EEW software processing is a minor factor in the overall delay.

Because magnitude computation can start with data from one station only, $\min(\overrightarrow{\Delta t_P} + \overrightarrow{\Delta t_w})$ is usually smaller than the time when a first location estimate is available (Δt_{origin}), except in the densest parts of the network.

Trigger Delays ($\overrightarrow{\Delta t_t}$)

The trigger delay describes the time it takes between the arrival of the P wave at the sensor and the detection of the trigger in the processing system. If measured in real time, it includes the data latency $\overrightarrow{\Delta t_l}$ and a small processing delay introduced by the triggering algorithm, in this case a short-term average/long-term average trigger (Allen, 1978). $\overrightarrow{\Delta t_t}$ is recorded routinely in the SeisComP3 system for every occurring trigger, so we have a dataset of $\overrightarrow{\Delta t_t}$ for Switzerland spanning almost two years. In California, we measured $\overrightarrow{\Delta t_t}$ during several weeks of real-time operations.

The similar shape of the trigger delay distribution (Fig. 4e) and the data latency distribution (Fig. 4a) indicates that $\Delta t_{t,i}$ at station i also is dominated by $\Delta t_{l,i}$. Similar behavior is seen in California, where the shapes of the distributions of data latencies (Fig. 4b) and of pick delays (Fig. 4f) are alike.

Depending on the location algorithm, delayed triggers may not only delay the computation of the first location estimate, but may also introduce errors in the location (e.g., if not-yet-arrived data or the arrival order are used to constrain the first location; Satriano *et al.*, 2008; Rosenberger, 2009). Optimizing $\overrightarrow{\Delta t_t}$ therefore will not only reduce alert times, but can also increase the accuracy of the first alert.

Associator Delay (Δt_a)

The associator delay is defined as the difference between the timestamps of the first earthquake location estimate and the last P-wave trigger. In Switzerland, this delay has been recorded routinely in real time by the SeisComP3 system, whereas for VS (EW) we measured Δt_a from offline playbacks of 119 events with magnitude ≥ 3.5 that occurred in southern California between January 2010 and August 2012.

Figure 4g shows the distribution of Δt_a for 289 events with a magnitude ≥ 1.5 that were located by the SeisComP3 installation. Half of the events were located within 0.7 s after the last P-wave trigger was created. For 16% of the events, however, the location process took more than 3.7 s. These longer delays are possibly due to increased load during real-time operation as they could not be reproduced in offline playbacks.

Δt_a in California is less than or equal to 1.0 s for 84% of the events using Earthworm's binder algorithm (Fig. 4h). Because we measured Δt_a from offline playbacks, we could not reproduce delays that may result from problems in the real-time processing.

Magnitude Estimation Time (Δt_m)

The magnitude estimation time is the time taken to find a magnitude consistent with the earthquake origin and the observed waveforms once a first origin and at least k seconds of envelope data from one of the first n stations are available ($k = 3$ and $n = 6$ for VS(SC3); $k = 1$ and $n = 4$ for VS (EW)). For VS(SC3), we measured this from offline playbacks of 97 events with a magnitude ≥ 2.5 that occurred in Switzerland and adjacent regions between January 2009 and June 2013. For VS(EW), we measured Δt_m from the same offline playbacks mentioned in the Associator Delay (Δt_a) section.

In VS(SC3), Δt_m is less than or equal to 1.1 s in 84% of the time and, like the associator delay (Δt_a), is therefore small compared with the delays of the other system components. Because of a slightly different optimization algorithm used in VS(EW), computation times are even faster with an 84th percentile of only 0.7 s (Fig. 4i,j).
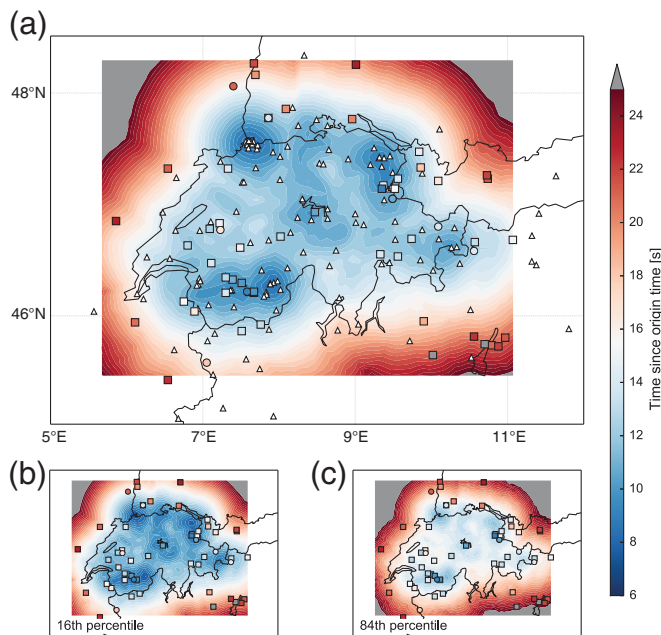
▲ **Figure 5.** Comparison between predicted and observed EEW performance in Switzerland. (a) The expected delay of the initial alert based on the observed delays of the system components is shown by the background color. Circles mark the locations of the nine events detected during real-time operations. Squares mark the locations of the 49 events used for the offline playbacks. First alert times are color coded. All events occurred between January 2009 and January 2014, had a magnitude ≥2.5, and were detected by the first six *P*-wave detections. White triangles mark the locations of broadband and strong-motion stations sending data in real time to the Swiss Seismological Service. (b,c) Similar to (a), but showing the 16th and 84th percentiles for the predicted delays.

USING OBSERVED DELAYS TO MODEL EXPECTED ALERT TIMES

Evaluating an EEW algorithm's performance solely on the basis of real-time earthquake detections has two major drawbacks: regions of poor performance may go unnoticed if there is lack of earthquakes in these areas during the testing phase, and a comparison between different EEW algorithms is only possible if they were operating at the same time on the same network.

We present a novel way to model performance by using equations (1.1) and (1.2) to combine the measured delays in the Delay Analysis section into a map of expected alert times. We demonstrate how this works in Switzerland and California for VS, but it could be extended to any algorithm and network. In principle, it is also applicable to an onsite algorithm by setting $\Delta t_{\mathrm{origin}} = 0$.

For each potential hypocenter (i.e., any point within the colored area in Figs. 5 and 6), we first compute the expected *P*-wave travel time to the *n* closest stations ($\overrightarrow{\Delta t_P}$; $n = 6$ for VS (SC3) and $n = 4$ for VS(EW); see the *P*-Wave Travel Time ($\overrightarrow{\Delta t_P}$) section), adding the values of trigger delays randomly
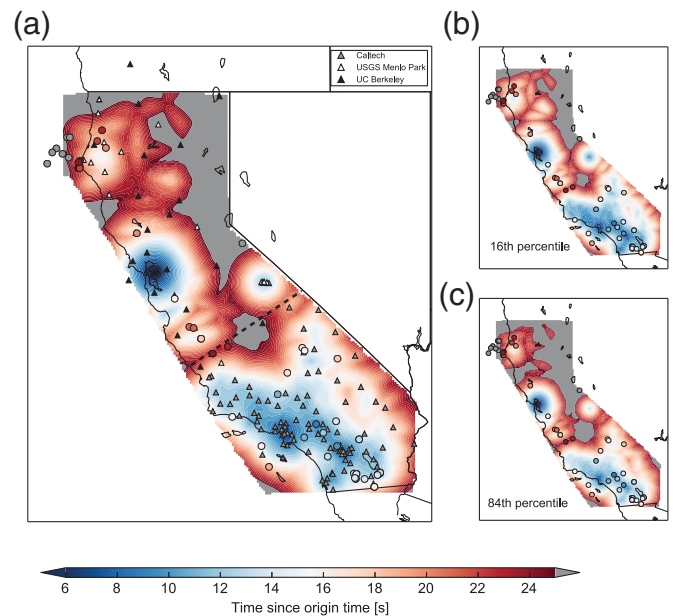
▲ **Figure 6.** Same as Figure 5 for California. Circles mark the locations of 56 events with a magnitude ≥3.5 that were correctly detected in real time between January 2012 and December 2013 White, gray, and black triangles mark locations of broadband stations sending data in real time and operated by the Californian seismic networks. The black dashed line marks the Gutenberg–Byerly line which roughly divides the seismic networks of northern and southern California.

drawn from the observed distributions of $\overrightarrow{\Delta t_t}$ (see the Trigger Delays ($\overrightarrow{\Delta t_t}$) section) for the particular set of stations. The sum of the maximum of these times and the associator delay, drawn from the distribution of Δt_a (see the Associator Delay (Δt_a) section), gives an estimate of when the first origin would be available ($\Delta t_{\mathrm{origin}}$; equation 1.1) for any of the potential hypocenters. The expected alert time is the sum of the time required to find a magnitude estimate (Δt_m; see the Magnitude Estimation Time (Δt_m) section) and either $\Delta t_{\mathrm{origin}}$ or the time when at least *k* seconds of envelope data from one of the *n* stations are available ($\overrightarrow{\Delta t_w}$; $k = 3$ for VS(SC3) and $k = 1$ for VS(EW); see the Waveform Delays ($\overrightarrow{\Delta t_w}$) section). Here again, values for $\overrightarrow{\Delta t_w}$ and Δt_m are drawn from their respective distributions. Because the delay distributions of the different system components cannot all be approximated by a standard functional form, no analytical solution exists to infer the percentiles of the final alert time distribution (Anjum and Perros, 2011). We repeated this analysis 500 times to infer the median, 16th, and 84th percentiles of the distribution of alert times for any hypothetical hypocenter. By choosing the 16th and 84th percentiles as the error bounds, 68% of the alert times fall within this range corresponding to a $\pm\sigma$ area if the alert times were normally distributed. To evaluate our model performance, we compared these values to the alert times observed

during real-time operations for seismicity that occurred within the model area (Figs. 5 and 6).

Because VS(SC3) has only been running for a few months, and seismicity in Switzerland is moderate, there are only a few real-time detections with a magnitude ≥ 2.5. We therefore extended the nine real-time observations with results from offline playbacks of waveforms from 49 events with magnitudes ≥ 2.5 between January 2009 and January 2014. To make these playbacks realistic, we delayed waveform packages by the median of the observed data latency ($\Delta t_{l,i}$; see the Data Latency $(\overrightarrow{\Delta t_l})$ section) at each station i. In Switzerland, 62% of the observed alert times fall within the 16th and 84th percentiles of the expected alert times (Fig. 5), which is in good agreement with the expected 68%. Within Switzerland, the best alert times vary from less than 12–13 s for the 16th percentile to around 14–18 s for the 84th percentile. Almost nowhere in Switzerland do we expect alert times with more than 19 s.

VS(EW) has been running for several years in real time, so we have sufficient real-time observations in California to evaluate our alert time predictions. Figure 6 shows the comparison of 56 events with magnitude ≥ 3.5 that occurred within California between January 2012 and December 2013 and were correctly detected by VS(EW) with four P-wave arrivals. Here only 43% of the observed alert times fall within the 16th and 84th percentiles of the expected alert times, with most alert times being longer. The main reasons are problems in detecting offshore events and glitches in the real-time system that seemed to have occurred more frequently in northern California than in southern California. Consequently, 67% of the alert times in southern California are within the 16th and 84th percentiles.

At the 16th percentile, alert times within the San Francisco Bay area and the Los Angeles basin are between 6–8 s and less than ∼14 s in most of southern California and those parts of northern California where the network is sufficiently dense. There is an ∼2 s difference between the 16th and 84th percentiles. In northern California, 16th percentile alert times increase to ≥ 25 s, reflecting the decrease of network density.

Our analysis is not a true evaluation of the networks in California, but merely a snapshot of them as seen by VS(EW) during the last two years. Recent developments have largely reduced the delay times for all stations in southern California that are equipped with modern dataloggers, and a statewide implementation of VS(EW) is now receiving real-time data streams from all Californian networks, reducing the alert times especially in central California.

In general, our model captures the main features of observed delay times, but because wave propagation effects, station noise levels, technical failures, and increased system load during larger earthquakes are not taken into account, discrepancies are expected. Further, changes of the network infrastructure between the observation and the simulation of alert times will also cause deviations from the expected alert times. Our analysis here indicates, however, that if the network is dense enough, these are only secondary effects relative to the fluctuations of time delays.
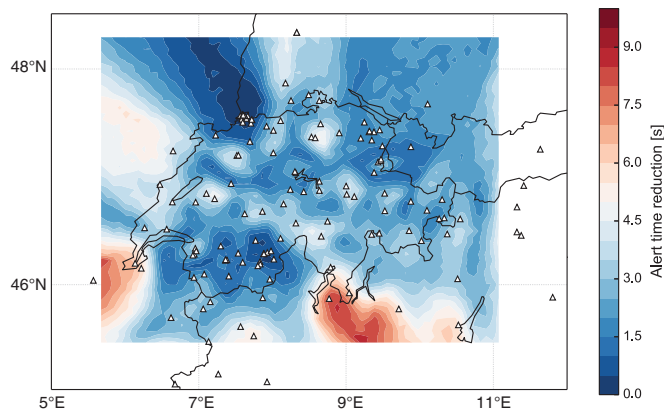
▲ **Figure 7.** Reduction of alert times by requiring two instead of six P-wave detections to compute a first location. Colors indicate the median reduction of alert times with respect to alert times presented in Figure 5a. Note that within Switzerland, hardly any improvement is seen in the densest parts of the network, whereas in less dense parts, alert times can be reduced by 5–6 s.

DISCUSSION AND CONCLUSIONS

It is crucial for any network operating or intending to operate EEW to understand the delays in providing the alerts. Our analysis, spanning two modern but very different dense seismic networks operating different hardware and software, gives an accurate evaluation of the time delays in VS(EW) and VS(SC3) and reveals the system components where algorithmic and infrastructural improvements would have the highest impacts. The most important contributing factors to the overall delays in the VS system are the data latency $(\overrightarrow{\Delta t_l})$ and the network density in combination with the number of P-wave detections necessary to make the first location $(\overrightarrow{\Delta t_P})$. For the two systems analyzed here, algorithm and hardware processing have only a minor effect on alert times. Beyond this somewhat obvious result, which we expect generalizes to many network-based EEW approaches, our methodology also allows us to compute the expected decrease in alert time for any improvements in network density $(\overrightarrow{\Delta t_P})$ and communication $(\overrightarrow{\Delta t_l})$ at any point within our region of interest. For example, Figure 7 shows the change in alert times for VS(SC3) if only two instead of six stations were required to compute the first location estimate. Although alert times in the densest part of the network would hardly change, such algorithmic improvements would lead to alerts in regions with larger station spacing being available 5–6 s earlier. In areas outside the network where alert times do not change significantly, P-wave travel times to the closest two stations are similar to those of the closest six stations. To improve alert times in these areas, station density has to be increased. For reduced alert times in the densest parts of the network, data latency $(\overrightarrow{\Delta t_l})$ and the required amount of waveform data to compute the magnitude $(\Delta t_{win}(k))$ would have to be reduced.
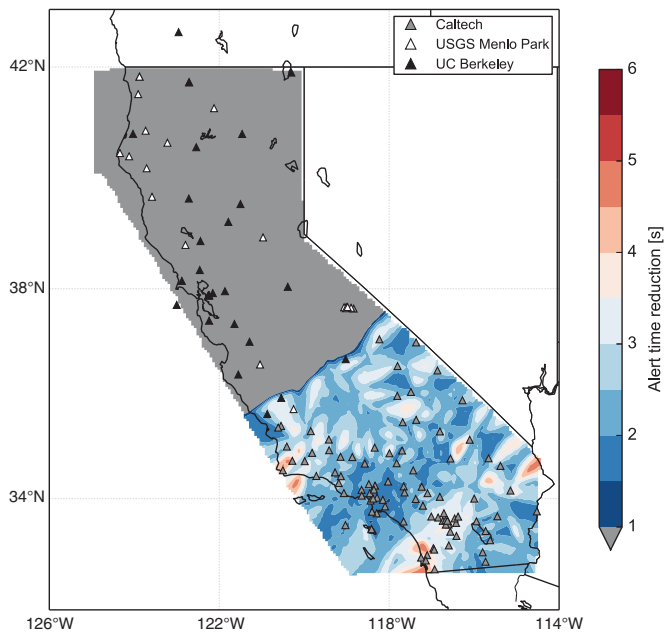
▲ Figure 8. Reduction of alert times by assuming shorter than currently observed data latencies of only 0.5–2.5 s for the southern California seismic network. Colors indicate the median reduction of alert times with respect to alert times presented in Figure 6a. Alert times change by up to 5 s in some parts of the network and by ~1 s in the Los Angeles basin.

A second example (Fig. 8) shows the change in alert times for events in southern California if we assume shorter data latencies and therefore shorter trigger delays ($\Delta t_{t,i}$ ranging between 0.5 and 2.5 s) than those presented in the Delay Analysis section for stations of the southern California seismic network. In some areas, alert times would be up to 5 s faster, whereas in the Los Angeles basin the median reduction would only be ~1 s.

Because any hardware and software optimization requires significant financial investments, our model could serve as an objective function to identify the most important seismic network upgrades or algorithmic improvements given a target alert time in a certain area.

We note that we do not address the accuracy of the alert, which is crucial for EEW, especially when considering faster algorithms to reduce alert times. Hence, a logical extension of our model is to also measure the time until an EEW alert reaches a certain accuracy. To compute this for any potential hypocenter would require the use of synthetic waveforms. Deterministic computation of realistic seismograms for 3D velocity structures at frequencies high enough to include the peak ground acceleration is currently limited by the necessary computation time and the resolution of 3D velocity models. Oth et al. (2010) used a statistical method to simulate seismograms and derived a method to systematically evaluate and optimize a network for EEW using the Istanbul EEW system as a case study. Zollo et al. (2009) applied the hybrid approach of Gallovič and Brokešová (2007), using deterministic and stat-

istical source modeling to compile a database of synthetic seismograms for the evaluation of the PRESTo EEW algorithm in southern Italy. Either of these approaches combined with the delay measurement described in this study could be the next step in evaluating EEW algorithm performances. §

REFERENCES

Allen, R. M. (2006). Probabilistic warning times for earthquake ground shaking in the San Francisco Bay area, *Seismol. Res. Lett.* **77,** no. 3, 371–376.

Allen, R. M. (2007). The ElarmS earthquake early warning methodology and application across California, in *Earthquake Early Warning Systems*, P. Gasparini, G. Manfredi, and J. Zschau (Editors), Springer-Verlag, Berlin, Germany, 21–43.

Allen, R. M., and H. Kanamori (2003). The potential for earthquake early warning in southern California, *Science* **300,** 786–789.

Allen, R. M., P. Gasparini, O. Kamigaichi, and M. Böse (2009). The status of earthquake early warning around the world: An introductory overview, *Seismol. Res. Lett.* **80,** no. 5, 682–693, doi: 10.1785/gssrl.80.5.682.

Allen, R. V. (1978). Automatic earthquake recognition and timing from single traces, *Bull. Seismol. Soc. Am.* **68,** no. 5, 1521–1532.

Anjum, B., and H. Perros (2011). Adding percentiles of Erlangian distributions, *IEEE Commun. Lett.* **15,** no. 3, 346–348, doi: 10.1109/LCOMM.2011.011011.102143.

Auclair, S., X. Goula, J.-A. Jara, and Y. Colom (2014). Feasibility and interest in earthquake early warning systems for areas of moderate seismicity: Case study for the Pyrenees, *Pure Appl. Geophys.*, doi: 10.1007/s00024-014-0957-x.

Beyreuther, M., R. Barsch, L. Krischer, T. Megies, Y. Behr, and J. Wassermann (2010). ObsPy: A Python toolbox for seismology, *Seismol. Res. Lett.* **81,** no. 3, 530–533, doi: 10.1785/gssrl.81.3.530.

Böse, M., E. Hauksson, K. Solanki, H. Kanamori, and T. H. Heaton (2009). Real-time testing of the on-site warning algorithm in southern California and its performance during the July 29 2008 M_w 5.4 Chino Hills earthquake, *Geophys. Res. Lett.* **36,** no. 3, 2–6, doi: 10.1029/2008GL036366.

Böse, M., E. Hauksson, K. Solanki, H. Kanamori, Y.-M. Wu, and T. H. Heaton (2009). A new trigger criterion for improved real-time performance of onsite earthquake early warning in southern California, *Bull. Seismol. Soc. Am.* **99,** no. 2A, 897–905, doi: 10.1785/0120080034.

Böse, M., R. Allen, H. Brown, G. Cua, M. Fischer, E. Hauksson, T. Heaton, M. Hellweg, M. Liukis, D. Neuhauser, and P. Maechling (2013). CISN ShakeAlert—An earthquake early warning demonstration system for California, in *Early Warning for Geological Disasters—Scientific Methods and Current Practice*, F. Wenzel and J. Zschau (Editors), Springer, Berlin, Germany.

Brown, H. M., R. M. Allen, M. Hellweg, O. Khainovski, D. Neuhauser, and A. Souf (2011). Development of the ElarmS methodology for earthquake early warning: Realtime application in California and

offline testing in Japan, *Soil Dyn. Earthq. Eng.* **31,** no. 2, 188–200, doi: 10.1016/j.soildyn.2010.03.008.

Cua, G. B., and T. H. Heaton (2007). The Virtual Seismologist (VS) method: A Bayesian approach to earthquake early warning, in *Earthquake Early Warning Systems*, P. Gasparini, G. Manfredi, and J. Zschau (Editors), Springer-Verlag, Berlin, Germany, 97–130.

Cua, G. B., M. Fischer, T. H. Heaton, and S. Wiemer (2009). Real-time performance of the Virtual Seismologist earthquake early warning algorithm in southern California, *Seismol. Res. Lett.* **80,** no. 5, 740–747, doi: 10.1785/gssrl.80.5.740.

Diehl, T., J. Clinton, T. Kraft, S. Husen, K. Plenkers, A. Guilhelm, Y. Behr, C. Cauzzi, P. Kästli, F. Haslinger, D. Fäh, C. Michel, and S. Wiemer (2013). Earthquakes in Switzerland and surrounding regions during 2012, *Swiss J. Geosci.* **106,** no. 3, 543–558, doi: 10.1007/s00015-013-0154-4.

Espinosa-Aranda, J. M., A. Jimenez, G. Ibarrola, F. Alcantar, A. Aguilar, M. Inostroza, and S. Maldonado (1995). Mexico City seismic alert system, *Seismol. Res. Lett.* **66,** no. 6, 42–53, doi: 10.1785/gssrl.66.6.42.

Fäh, D., D. Giardini, P. Kästli, N. Deichmann, M. Gisler, G. Schwarz-Zanetti, S. Alvarez-Rubio, S. Sellami, B. Edwards, B. Allmann, F. Bethmann, J. Wössner, G. Gassner-Stamm, S. Fritsche, and D. Eberhard (2011). *ECOS-09 Earthquake Catalogue of Switzerland Release 2011.*

Gallovič, F., and J. Brokešová (2007). Hybrid k-squared source model for strong ground motion simulations: Introduction, *Phys. Earth Planet. In.* **160,** no. 1, 34–50, doi: 10.1016/j.pepi.2006.09.002.

Gerstenberger, M. C., S. Wiemer, L. M. Jones, and P. A. Reasenberg (2005). Real-time forecasts of tomorrow's earthquakes in California, *Nature* **435,** no. 7040, 328–331, doi: 10.1038/nature03622.

Hanka, W., J. Saul, B. Weber, J. Becker, and P. Harjadi (2010). Real-time earthquake monitoring for tsunami warning in the Indian Ocean and beyond, *Nat. Hazards Earth Syst. Sci.* **10,** no. 12, 2611–2622, doi: 10.5194/nhess-10-2611-2010.

Heaton, T. H. (1985). A model for a seismic computerized alert network, *Science* **228,** 987–990.

Hoshiba, M., O. Kamigaichi, M. Saito, S. Tsukada, and N. Hamada (2008). Earthquake early warning starts nationwide in Japan, *Eos Trans. AGU* **89,** no. 8, 73, doi: 10.1029/2008EO080001.

Housner, G. W., L. A. Bergman, T. K. Caughey, A. G. Chassiakos, R. O. Claus, S. F. Masri, R. E. Skelton, T. T. Soong, B. F. Spencer, and J. T. P. Yao (1997). Structural control: Past, present, and future, *J. Eng. Mech.* **123,** no. 9, 897–971, doi: 10.1061/(ASCE)0733-9399(1997)123:9(897).

Hsiao, N.-C., Y.-M. Wu, L. Zhao, D.-Y. Chen, W.-T. Huang, K.-H. Kuo, T.-C. Shin, and P.-L. Leu (2011). A new prototype system for earthquake early warning in Taiwan, *Soil Dyn. Earthq. Eng.* **31,** no. 2, 201–208, doi: 10.1016/j.soildyn.2010.01.008.

Hunter, J. D. (2007). Matplotlib: A 2D graphics environment, *Comput. Sci. Eng.* **9,** no. 3, 90–95, doi: 10.1109/MCSE.2007.55.

Kanamori, H. (2005). Real-time seismology and earthquake damage mitigation, *Annu. Rev. Earth Planet. Sci.* **33,** no. 1, 195–214, doi: 10.1146/annurev.earth.33.092203.122626.

Kuyuk, H. S., and R. M. Allen (2013). Optimal seismic network density for earthquake early warning: A case study from California, *Seismol. Res. Lett.* **84,** no. 6, 946–954, doi: 10.1785/0220130043.

Kuyuk, H. S., R. M. Allen, H. M. Brown, M. Hellweg, I. Henson, and D. Neuhauser (2014). Designing a network-based earthquake early warning algorithm for California: ElarmS-2, *Bull. Seismol. Soc. Am.* **104,** no. 1, 162–173, doi: 10.1785/0120130146.

Mărmureanu, A., C. Ionescu, and C. O. Cioflan (2011). Advanced real-time acquisition of the Vrancea earthquake early warning system, *Soil Dyn. Earthq. Eng.* **31,** no. 2, 163–169, doi: 10.1016/j.soildyn.2010.10.002.

Nakamura, Y. (1988). On the urgent earthquake detection and alarm system (UrEDAS), in *Proc. Ninth World Conference on Earthquake Engineering*, Tokyo-Kyoto, Japan, 2–9 August.

Nakamura, Y., J. Saita, and T. Sato (2011). On an earthquake early warning system (EEW) and its applications, *Soil Dyn. Earthq. Eng.* **31,** no. 2, 127–136, doi: 10.1016/j.soildyn.2010.04.012.

Oth, A., M. Böse, F. Wenzel, N. Köhler, and M. Erdik (2010). Evaluation and optimization of seismic networks and algorithms for earthquake early warning—the case of Istanbul (Turkey), *J. Geophys. Res.* **115,** no. B10, doi: 10.1029/2010JB007447.

Rosenberger, A. (2009). Arrival-time order location revisited, *Bull. Seismol. Soc. Am.* **99,** no. 3, 2027–2034, doi: 10.1785/0120080270.

Satriano, C., L. Elia, C. Martino, M. Lancieri, A. Zollo, and G. Iannaccone (2011). PRESTo, the earthquake early warning system for southern Italy: Concepts, capabilities and future perspectives, *Soil Dyn. Earthq. Eng.* **31,** no. 2, 137–153, doi: 10.1016/j.soildyn.2010.06.008.

Satriano, C., A. Lomax, and A. Zollo (2008). Real-time evolutionary earthquake location for seismic early warning, *Bull. Seismol. Soc. Am.* **98,** no. 3, 1482–1494, doi: 10.1785/0120060159.

Steim, J. M., and R. D. Reimiller (2014). Timeliness of data delivery from Q330 systems, *Seismol. Res. Lett.* **85,** no. 4, 844–851, doi: 10.1785/0220120170.

Wald, D. J., V. Quitoriano, T. H. Heaton, H. Kanamori, C. W. Scrivner, and C. B. Worden (1999). TriNet "ShakeMaps": Rapid generation of peak ground motion and intensity maps for earthquakes in southern California, *Earthq. Spectra* **15,** no. 3, 537–555, doi: 10.1193/1.1586057.

Wu, Y.-M., H. Kanamori, R. M. Allen, and E. Hauksson (2007). Determination of earthquake early warning parameters, τ_c and P_d, for southern California, *Geophys. J. Int.* **170,** no. 2, 711–717, doi: 10.1111/j.1365-246X.2007.03430.x.

Zollo, A., Iannaccone, G., M. Lancieri, L. Cantore, V. Convertito, A. Emolo, G. Festa, F. Gallovič, M. Vassallo, C. Martino, C. Satriano, and P. Gasparini (2009). Earthquake early warning system in southern Italy: Methodologies and performance evaluation, *Geophys. Res. Lett.* **36,** no. 4, 1–6, doi: 10.1029/2008GL036689.

Zollo, A., S. Colombelli, L. Elia, A. Emolo, G. Festa, G. Iannaccone, C. Martino, and P. Gasperini (2013). An integrated regional and on-site earthquake early warning system for southern Italy: Concepts, methodologies and performances, in *Early Warning for Geological Disasters—Scientific Methods and Current Practice*, J. Z. Friedemann Wenzel (Editor), Springer, Berlin, Germany, 117–138.

Yannik Behr
John Clinton
Philipp Kästli
Carlo Cauzzi
Roman Racine
Men-Andrin Meier
Swiss Seismological Service
ETH Zürich
Sonneggstrasse 5
8092 Zürich, Switzerland
behr@sed.ethz.ch

Published Online 15 April 2015